Fire Safety Journal 125 (2021) 103430

Contents lists available at ScienceDirect

Fire Safety Journal

journal homepage: www.elsevier.com/locate/firesaf

Opposed flame spread over thick solid fuels under influence of sub-atmospheric pressure and low-velocity flow

Feng Zhu [a], Shuangfeng Wang [a,b,c,*], Zhanbin Lu [d], Chuanjia Wu [a,c]

[a] Key Laboratory of Microgravity, Institute of Mechanics, Chinese Academy of Sciences, Beijing, 100190, China
[b] State Key Laboratory of High-Temperature Gas Dynamics, Chinese Academy of Sciences, Beijing, 100190, China
[c] School of Engineering Science, University of Chinese Academy of Sciences, Beijing, 100049, China
[d] Institute of Applied Mathematics and Mechanics, Shanghai University, Shanghai, 200072, China

ARTICLE INFO

Keywords:
Sub-atmospheric pressure
Low-velocity flow
Flame spread
Solid
Flammability

ABSTRACT

The future generation of inhabited spacecraft will have a significantly different cabin environment from the present ones, characterized by low pressure and elevated oxygen concentration. This new atmosphere and the low-velocity gas flows in microgravity provide distinct conditions for the combustion of the solid materials used, and their influence on material flammability is of particular interest in the fire safety of spacecraft. Experiments have been conducted to investigate the effects of sub-atmospheric pressure and low flow velocity on the opposed flame spread and extinction behaviors over a thick PMMA. A flammability map was constructed that delineates the uniform regime, the flamelet regime, and extinction limits for thick PMMA under sub-atmospheric pressures. The limiting oxygen concentration increases with the reduced ambient pressure at a fixed opposed flow, while the flamelet regime becomes wider. Under low ambient pressure, the flame spread rate increases with the flow velocity, but the increasing rate slows down. At a constant oxygen concentration, the flame spread rate increases with the ambient pressure and gas-phase conduction dominates flame spread. At a constant oxygen partial pressure, the higher ignition temperature and less gas-phase conduction reduce the flame spread rate synchronously with the increased pressure.

1. Introduction

Flame spread behaviors over solid materials depend strongly on environmental conditions. Because of the significantly different environment in a spacecraft than Earth, the flame spread has been of interest for spacecraft fire safety for several decades (e.g., the reviews of T'ien et al. [1] and Fujita [2]). To reduce the risk of decompression sickness during extra-vehicular activities (EVA), and reduce the time required to pre-breath for EVA preparation, the ambient pressure proposed by NASA inside the next generation of space vehicles is 52.7–58.6 kPa with an oxygen concentration of 30–34% by volume [3,4]. The cabin environment of the Chinese Lunar Lander is suggested with a pressure of (58 ± 4) kPa with an oxygen partial pressure of (21 ± 2) kPa [5]. These new atmospheric conditions, together with the low-velocity gas flows that are induced under microgravity by the heating and ventilation systems, constitute the unique environments for the combustion of the solid materials onboard. It is therefore important to have the information on how slow gas flows at low-pressure influence flame spread behaviors and consequently material flammability.

Experiments conducted in normal gravity on flame spread over thick solid fuel with the buoyant flow have shown an exponentially increase with the ambient pressure [6–9] and the exponent of pressure increases with the sample thickness [9]. In normal gravity downward flame spread, as the ambient pressure is reduced, the buoyant flow velocity decreases, resulting in the increase of the residence time for the gas mixture in the flow. Meanwhile, the chemical time for second-order kinetics is inversely proportional to pressure, and, the finite-rate effects should depress the spread rate at low pressures [10,11]. However, the Damköhler number, which is defined as the ratio of the residence time to the chemical time is expected to decrease, causing the finite-rate effects to reduce the spread rate [10]. It is noted that the influence of the opposed flow on flame spread behavior is implied in the influence of the ambient pressure, then the effect of oxidizer flow velocity cannot be investigated as a separate parameter. In addition, the low-velocity environment, which is induced by the spacecraft ventilation system, cannot be obtained in the open environment on the ground. Due to the long-timescale for thermally thick solid burning, it is difficult to perform

* Corresponding author. 15 Bei-Si-Huan-Xi Road, Institute of Mechanics, Chinese Academy of Sciences, Beijing, China.
E-mail address: sfwang@imech.ac.cn (S. Wang).

https://doi.org/10.1016/j.firesaf.2021.103430
Received 16 April 2021; Received in revised form 11 July 2021; Accepted 19 August 2021
Available online 23 August 2021
0379-7112/

Nomenclature

Symbols

C_1	constant
C_2	constant
c_s	solid specific heat (kJ/kg/K)
c_{pg}	gas specific heat (kJ/kg/K)
Gr	Grashof number (−)
H_c	height of the narrow channel (mm)
l	characteristic length (m)
l_h	solid heating length ahead of the pyrolysis front (m)
P	pressure (kPa)
P_{O2}	oxygen partial pressure (kPa)
Pr	Prandtl number (−)
$\dot{q}''_{fc}$	conductive heat flux from the flame leading edge to the solid (kW/m^2)
r	stoichiometric mass ratio between oxygen and fuel (−)
Re	Reynolds number (−)
t_{ig}	ignition delay time (s)
T_f	characteristic flame temperature (K)
T_∞	ambient pressure (K)
V_f	flame spread rate (m/s)
V_g	opposed flow velocity (m/s)
x	coordinate axis (m)
X_{O2}	oxygen concentration in volume (−)
Y_{O2}	oxygen mass fraction (−)

Greek

λ_g	gas-phase conductivity (W/m/K)
λ_s	fuel conductivity (W/m/K)
ρ_g	gas density (kg/m^3)
ρ_s	fuel density (kg/m^3)
Δh_c	heat of combustion (MJ/kg)

experiments in the microgravity environment using ground-based apparatus such as the drop tower, and it is merely and expensive to carry out experiments in space where it can provide a long duration microgravity environment. Previous microgravity experiments were mainly focused on the effect of flow velocity and oxygen concentration on flame spread behavior and flammability limit at standard atmosphere [12–15]. The effect of ambient pressure on flame spread behavior is scarce [16,17], and there are limited studies on the effect of pressure with the low-velocity flow on the flame spread and extinction behavior over solid fuel.

With the low-velocity flow, particularly at near-limiting conditions, the initially uniform flame front breaks into separate flamelets and propagates individually to form a fingering pattern on the fuel surface due to the diffusive-thermal instability [13,18–21]. This fingering flame spread is persistent and able to extend the flammability of solid fuel [13], thus, it is important for fire safety prevention in practice. Uchida et al. [22] and Matsuoka et al. [19] used an effective Lewis number which is defined as the ratio of the effective thermal diffusivity to the oxygen diffusivity, to clarify the effect of thermal-diffusivity on the formation of fingering pattern. When the ambient pressure is reduced, the mass diffusivity of oxygen into the bulk mixture will be increased, then the Lewis number is different from that at standard atmosphere. Whether a flame/flamelet can survive under sub-atmospheric environment with low-velocity flow is information crucial in order to reduce the probability of a fire.

This work presents experiments conducted to study the effect of sub-atmospheric pressure and low-velocity oxidizer flow on flame spread behaviors over thermally thick solid and extinction characteristics in an opposing gas flow. The experimental setup was composed of a narrow channel apparatus and a containment chamber, with the former producing the intended flow velocities, and the latter allowing a range of ambient pressures and oxygen concentrations. It is worth noting that the narrow-channel type apparatus is an alternative method to suppress the buoyant flow, and this apparatus has been widely used to capture the essential features of microgravity flame spread [23–29]. Particularly, such an apparatus provides an abundant test time that is needed in the experiments of flame spread over thermally-thick fuels. Flammability maps and flame spread mode under low-pressure using gas flow velocity and oxygen concentration as coordinates are presented. The effects of ambient pressure and gas flow velocity on flame spread mode, flame spread rate, and flame extinction limit are analyzed.

2. Experiment

A schematic diagram of the experimental setup is illustrated in Fig. 1.

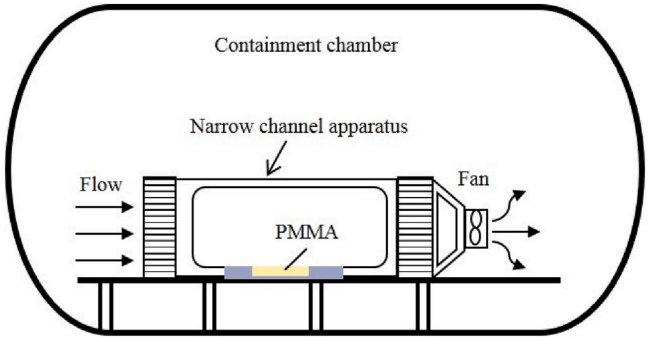

Fig. 1. Schematic diagram of the experimental setup.

It consists of a containment chamber and a narrow channel apparatus. The containment chamber is a cylindrical pressure vessel with an inner diameter of 600 mm, and a length of 920 mm, with an inner volume of 260 L. It consists of one port at the back for electrical connection and gas inlet and outlet, two fans, and three SiO_2 windows installed on the front, left, and right sides for observation purposes. The desired oxygen concentration is achieved by pumping the air out from the chamber to preset pressure and adding pure oxygen/nitrogen into the chamber until the mixture inside the chamber finally reaches the desired pressure. To ensure good mixing, two fans placed at the front and back of the chamber are turned on for at least 8 min for mixing. The internal pressure and oxygen concentration of the chamber are monitored by a pressure transducer and an oxygen sensor respectively. The ambient temperature inside the chamber is monitored with a K-type thermocouple installed near the sample holder to guarantee that the chamber does not heat excessively during the tests. The measured results showed that the maximum recorded temperature increase is 2 K, and the variation of pressure and oxygen concentration has little changes.

A horizontal channel apparatus that is 410 mm long and 164 mm wide, and an adjustable height H_c for different ambient pressures is used inside the chamber. The inlet of the channel is filled with an aluminum honeycomb to ensure a uniform gas flow. A fan is fixed at the end of the channel to generate the flow velocity in the range of 0–40 cm/s through varying the voltage. The flow velocity is calibrated by laser particle velocimetry (LDV). The reduced buoyancy can be characterized by the Grashof number (Gr), and experiments have been shown that when $GrPr < 2000$, the gas-phase heat transfer is the dominant mechanism, and the heat transfer through buoyancy is sufficiently weak [30]. We followed

with Wang et al. [31], Xiao et al. [25], Hossian et al. [23], and Pepper et al. [32] who have done the same practice. In this work, three ambient pressures were used, i.e. 101 kPa, 58 kPa, and 35 kPa, and the corresponded channel heights are 5 mm, 7 mm, and 10 mm respectively, which is in accordance with that used by Wang et al. [31]. The flame spread behavior under 101 kPa is desirable as a reference benchmark.

The fuel used in experiments is a 10 mm thick polymethylmethacrylate (PMMA) plate, measuring 60 mm long by 50 mm wide, with a density of 1.19 g/cm^3. As schematically shown in Fig. 2, the fuel sample is embedded in the aluminum floor of the test section, with its top face flushed with the sample holder and the side and bottom faces insulated from the floor. A resistively heated coil of ignition wire is embedded 5 mm from the downstream end of the sample in experiments. The fuel sample is ignited with a power of 165 W.

Two series of tests are performed to explore the effect of reduced ambient pressure and the oxidizer flow velocity on flame spread over thermally-thick solid. In the first series of tests, the ambient pressure is 101 kPa, 58 kPa, and 35 kPa, respectively, and the opposed flow velocity is varied from 40 cm/s to the lowest velocity at which flame spread cannot be sustained while the oxygen concentration is fixed. In the second series, the oxygen partial pressure (P_{O2}) is fixed at 21.3 kPa. During each test, the desired pressure and oxygen concentration are initiated first and are allowed to fully mix within the chamber. Thereafter, the fan at the back of the channel is switched on to form the desired flow velocity. After the opposed flow is uniform, the sample will be ignited by heating wire. Each test is recorded with two different cameras: A Nikon D7200 with a resolution of 1920 × 1080 pixels at 25 fps from the side view, and a Sony DCR-TRV900E with a resolution of 1440 × 1080 pixels at 25 fps from the top view. Different camera settings were used to record the flame spread for different test cases since the flame luminosities vary significantly. Under each flow velocity, if the flame extinguishes when it spreads forward less than 20 mm away from the igniter, the corresponding oxygen concentration is defined as the limiting oxygen concentration. To ensure the experimental repeatability and obtain an average value, all tests are repeated at least three times. The opposed flame spread process is steady, and the highest standard deviation of flame spread rate between comparable tests is about 8%.

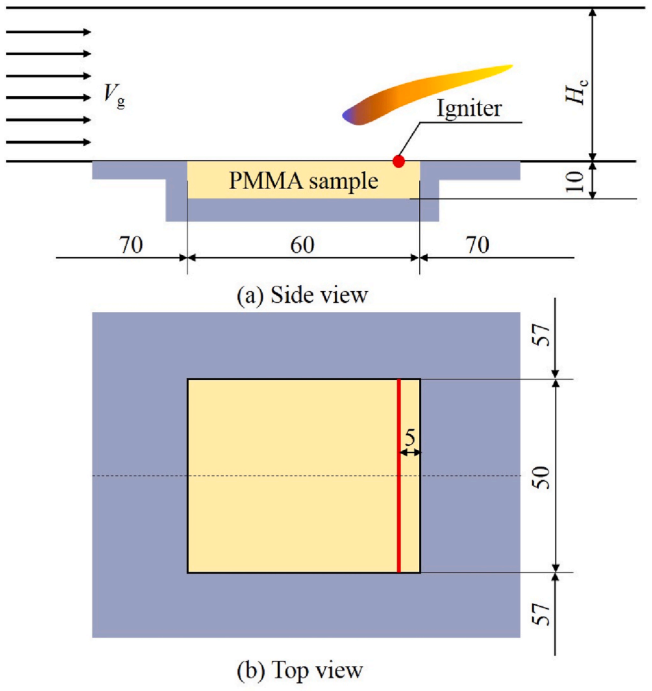

Fig. 2. Schematic diagrams showing the side and top view of the test section. All dimensions are in millimeters.

3. Results and discussion

3.1. Flammability map and flame spread modes

Within the flammability range, two flame modes are observed with the variation of low-velocity flow and/or oxygen concentration under constant pressure, that is uniform flame and flamelet. Typical flame images under $P = 35$ kPa, 58 kPa and $P_{O2} = 21.3$ kPa are shown in Fig. 3. Under low pressure, the flame is always blue-colored for all the flow velocities, and the color becomes diluted as the oxygen concentration decreases. It is evident that at high-velocity flow, the flame front is uniform, while the flow velocity is lowered to the critical value, $V_{g,cr}$, the continuous flame front shrinks and becomes corrugated, and at the end, the uniform flame separates into flamelets. The corresponding $V_{g,cr}$ increases for the formation of flamelet as the pressure is reduced. For example, $P = 58$ kPa, $V_{g,cr} \approx 7$ cm/s, and when $P = 35$ kPa, $V_{g,cr} \approx 15$ cm/s.

Under $P_{O2} = 21.3$ kPa, when the flow velocity is 20 cm/s, the color of the flame shows that soot formation processes become more significant as the ambient pressure is increased as shown in Fig. 3c. Specifically, under lower ambient pressure, the flame is blue-colored with a bright white core in the middle part of the flame. It indicates that as the reduced ambient pressure increases the oxygen concentration in volume, the increased oxygen concentration promotes the solid combustion process. Under $P = 101$ kPa, when the oxidizer flow velocity is lower than $V_{g,cr}$ (≈8 cm/s), steady flame propagation cannot occur. When $V_g > 8$ cm/s, the flame leading edge is uniform. A three-dimensional flame with a width of approximately two-thirds of the sample width develops with low-velocity oxidizer flow. With the increase of the flow velocity, a two-dimensional flame develops with an increase in brightness. When $V_g = 20$ cm/s, the tail of the flame becomes yellow, and the flame length increases. Under $P = 58$ kPa, when $V_g \leq 10$ cm/s, an increasing number and decreasing sizes of flamelets can be observed. However, under $P = 35$ kPa, three flamelets were formed when $V_g = 9$ and 10 cm/s. As decreasing the flow velocity further, only two flamelets were formed and adhered to the sides of the sample. It is implied that the variation of the number and size of the flamelet is not straightforward.

The flame spread modes at three different ambient pressures are visualized by the flammability map shown in Fig. 4. Under each ambient pressure, three regimes can be identified on the entire X_{O2} - V_g plane, namely a uniform flame regime where the flame leading edge is continuous along the transverse direction, a flamelet regime where the flame takes the spread forward in the form of transversely distributed, isolated flamelets, and an extinguished regime. Under the high ambient pressure environment, the flame can spread forward in lower oxygen concentration and/or lower velocity flow, i.e. the flammable range of the material becomes wider, however, the flamelet regime becomes wider as the pressure decreases. In addition, for all the ambient pressures, the flamelet regime shrinks with the increased flow velocity, and when the flow velocity increases to a critical value, the flamelet regime disappears. This result indicates that the three-dimensional flamelet can survive in low-pressure, and the possibility of the undetectable fire hazard may be increased due to the wider flamelet regime under a sub-atmospheric pressure environment.

The fingering pattern of flame identified above occurs exclusively near the quenching limit, where radiative heat loss plays an important role. For opposed flame spread over thick solid PMMA plates under a standard atmospheric environment, the formation of flamelets has been observed by Matsuoka et al. [19] in a normal-gravity environment and by Zhu et al. [13] in a microgravity environment, and diffusive–thermal nature of the instability associated with the formation of flamelets in both experiments. Analysis shows that a critical effective Lewis number can be used to clarify the uniform flame and flamelet, and both mass and heat transfer involves the flame separation phenomenon [13,19]. In addition, for near-quenching-limit opposed-flow smolder spread over thin solid fuels, the characteristic width of the fingers developed after

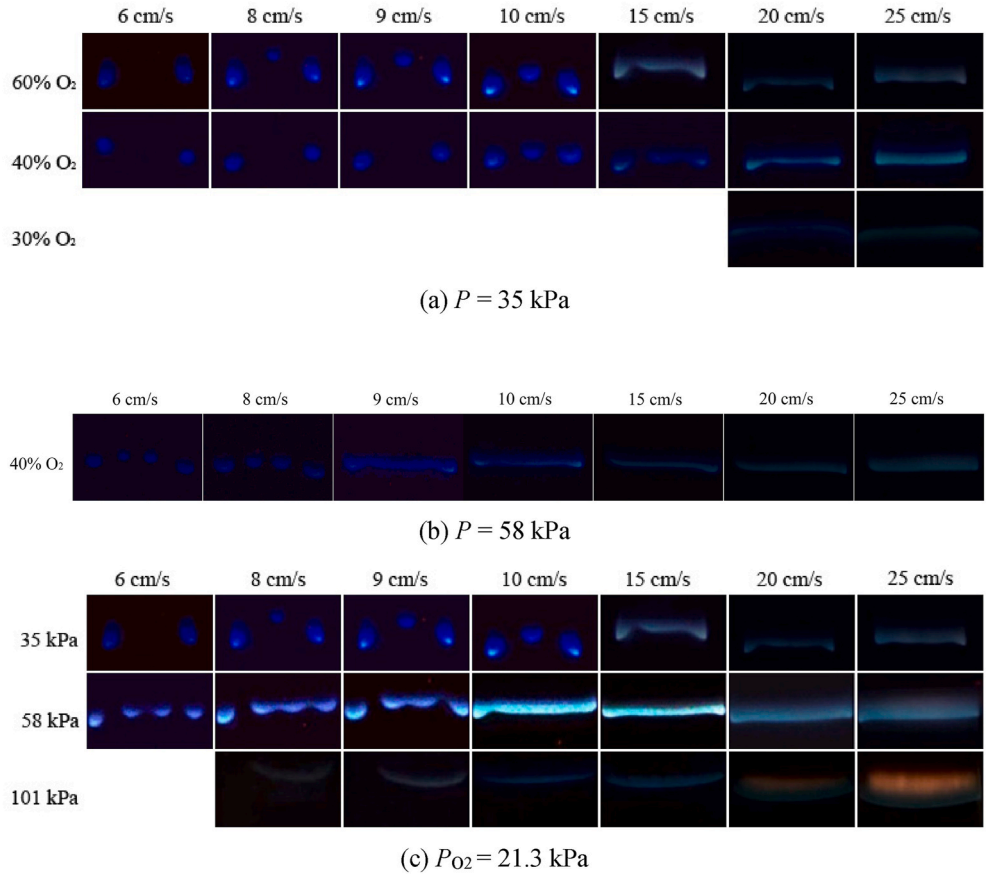

Fig. 3. Flame images illustrating steady-state flame spread at different pressures and flow velocities.

the onset of instability is well correlated with the heat loss intensity, whereas the characteristic separation distance between neighboring fingers is correlated with the Peclet number of the gas flow [33]. It is expected that under a sub-atmospheric environment, the variation of the thermal-diffusive instability may be applied to the characterization of the flamelets identified in the present experiment.

3.2. Effect of ambient pressure on flame spread rate

Flame spread rates are determined from the recorded images for each test. The positions of flame and flamelet leading edges are tracked frame by frame. The flame spread rates are determined by linearly fitting the evolution curve. For the uniform flame, the position of the leading edge is tracked along the centerline. For flamelets, the average of each flamelet spread rate is used for comparison. The variation of flame spread rate with ambient pressure at 40% O_2 is shown in Fig. 5a. It is seen that under constant oxygen concentration and flow velocity, the flame spread rate decreases as the pressure is reduced. At $V_g = 20$ cm/s, the flame spread rate under $P = 35$ kPa is 72% lower than that under $P = 101$ kPa. Of more relevance to future space exploration, however, are normoxic conditions where the partial pressure of oxygen conditions (rather than oxygen mole fraction) is held constant at the same level as normal atmospheric air. The variation of flame spread rate with ambient pressure at $P_{O2} = 21$ kPa is shown in Fig. 5b. As environments are changed to reduced ambient pressure and increased oxygen concentration, the flame spread rate increases, showing an opposite trend with that at a constant oxygen concentration. The total reduction in the flame spread rate is about 90% between standard air condition and the normoxic atmosphere at 35 kPa for all the opposed flow velocities. It indicates that the fire risk increases under a high oxygen concentration environment with low pressure.

3.3. Effect of oxidizer flow velocity on flame spread rate

Fig. 6 shows the flame spread rates obtained from the NCA experiments, and the microgravity flame spread rates with low-velocity flow [12,13], as well as higher flow experiments on Earth [34] at $P = 101$ kPa under different oxygen concentrations. The variation of flame spread rate with the flow velocity in the NCA agrees well with the microgravity data at lower flow rates, indicating that buoyancy is effectively suppressed. In the low-velocity regime, the flame spread rates are sensitive to very low-velocity flows, similar to the case for thermally thin fuels [35] and plastic rods [14]. In this regime, radiation heat loss controls the flame spread behavior [13,36]. In the medium-velocity regime, the flame spread rate increases with increasing flow slowly, and heat transfer dominates the flame spread. In the high-velocity regime, the flame spread rate decreases with the increased flow until the flame extinguishes, where the chemical kinetics dominates the flame spread [34]. The data of flame spread rate in low-velocity flow complete the flame spread map in the whole flammability regime.

The variation trend of flame spread rate with opposed gas flow velocity under sub-atmospheric pressure is similar to that under $P = 101$ kPa. The flame spread rates as a function of gas flow velocity under $P = 58$ kPa and 35 kPa are shown in Fig. 7a and Fig. 7b. It is clear that flame spread rate first increases with the increased flow by a large margin, and then the increasing rate becomes slow. This is the first time to give the flame spread rate for thermally thick solid fuel under low ambient pressure with the low-velocity opposed gas flow. The variation of flame spread rate with the opposed flow velocity for the cases where pressure is the normoxic equivalent for each specific oxygen percentage is presented in Fig. 7c. Under $P = 35$ kPa and 58 kPa, there is a significant difference in the slop of the flame spread rate with the opposed flow velocity between the radiation-controlled regime and thermal regime in

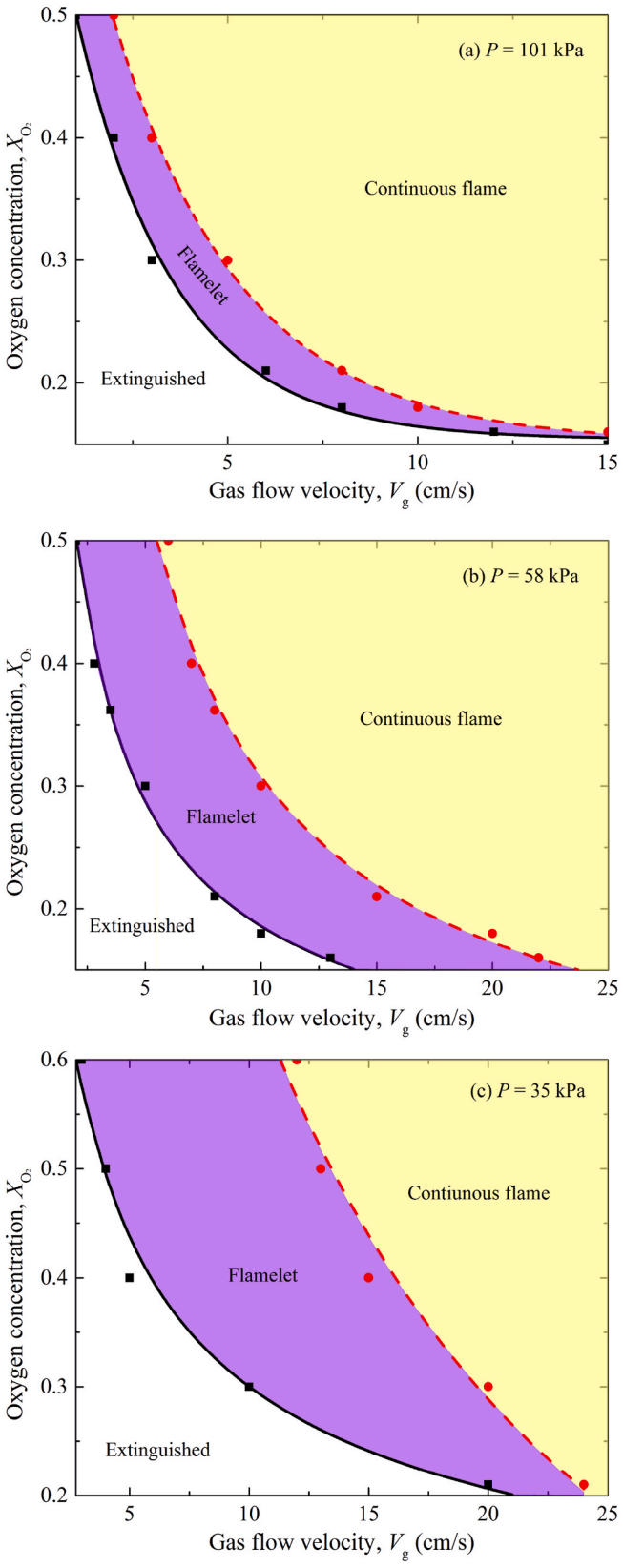

Fig. 4. Flammability map showing the distribution of spread modes and flame extinction limit on the X_{O2}-V_g plane under different ambient pressures.

the flow velocity range of 0–80 cm/s. Comparatively, at 40% O_2, under 101 kPa, the transition flow velocity is about 10 cm/s, while under 58 kPa, the transition flow velocity is about 30 cm/s, and when the ambient pressure is reduced to 35 kPa, the transition flow velocity is about 40 cm/s, implying that the transition flow velocity increases with the reduced ambient pressure. The effect of ambient pressure on flame spread rate will be discussed in detail in the Discussion section.

3.4. Discussion

In the analysis of the effect of ambient pressure on flame spread rate, the flame spread process can be treated as a series of ignition steps where the flame acts both as the heating source of solid pyrolysis and the piloted ignition [3,37–39]. The opposed flame spread rate can be obtained from the ratio of the solid heating length ahead of the pyrolysis front (l_h) and the ignition time (t_{ig}) *i.e.* $V_f = l_h/t_{ig}$. As indicated in this discussion section, only the experiments conducted away from limiting conditions are discussed, and the spread rate is primarily dominated by the heat transfer term. For a thick solid, the ignition delay time can be estimated as

$$t_{ig} = \frac{\pi}{4}\lambda_s \rho_s c_s \left(\frac{T_{ig} - T_\infty}{\dot{q}''_{fc}}\right)^2 \tag{1}$$

$$\dot{q}''_{fc} = C_1 \left(\lambda_g \rho_g c_{pg} V_g / x\right)^{1/2} \left(T_f - T_{ig}\right) \tag{2}$$

where λ, ρ, and c are the conductivity, density, and specific heat. The subscripts "s" and "g" refer to the solid and gas phase, respectively. T_{ig} and T_∞ are the ignition and initial temperature of the solid, T_f is the flame temperature. V_g is the gas flow velocity, C_1 is constant. From the Ref. [3,38], l_h is proportional to the boundary layer thickness, that is $l_h \propto lRe_l^{-1/2} = C_2 V_g^{-1/2}$, where l is a characteristic length, C_2 is constant. Considering that the buoyant flow is suppressed sufficiently, l_h can be taken as constant under a constant flow velocity. At a constant flow velocity, the heat conduction from the flame leading edge to the solid $\dot{q}''_{fc}$ is mainly affected by the temperature gradient $T_f - T_{ig}$. This temperature difference can be approximated by Ref. [37].

$$T_f - T_{ig} = \frac{Y_{O_2} \Delta h_c}{c_{pg} r} \tag{3}$$

where Y_{O_2} is the oxygen mass fraction, Δh_c is the heat of combustion, and r is the stoichiometric mass ratio between oxygen and fuel.

The ambient pressure may affect the flame spread rate by changing the ignition temperature T_{ig} and the heat flux from the flame to the solid $\dot{q}''_{fc}$. Under a constant oxygen volume concentration, the studies by McAllister et al. [40] showed that when the external radiant heat flux and opposed flow velocity V_g are fixed, as the ambient pressure is reduced, the ignition temperature decreases, as with the ignition delay time. It is noted that the ignition delay time increases with the ambient pressure in both constant oxygen concentration and oxygen partial pressure environments. It is seen that both the ignition temperature and flame heat flux dominates the flame spread rate, Then the effect of ambient pressure on the heat flux from the flame to the solid $\dot{q}''_{fc}$ so as to the flame spread rate is discussed in the following.

3.4.1. Flame spread at a constant oxygen concentration

At a constant oxygen concentration, Y_{O_2} is constant. c_{pg}, r and Δh_c are all insensitive to the ambient pressure [30], and thus $T_f - T_{ig}$ will be evaluated as the constant value. Considering that $\rho_g \sim P$, $\dot{q}''_{fc} \sim P^{1/2}$, $t_{ig} \sim P^{-1}$ and $V_f \sim P$. Then, it is deduced that V_f will increase with the increased ambient pressure. The reduction in the ignition temperature is competing with the increase in the heat flux from the flame to the solid

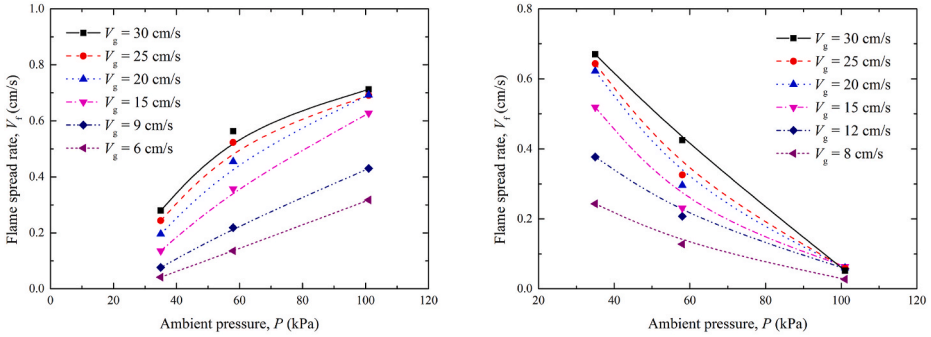

(a) 40% O_2 (b) P_{O2} = 21 kPa

Fig. 5. Variation of flame spread rate with ambient pressure under different opposed flow velocities.

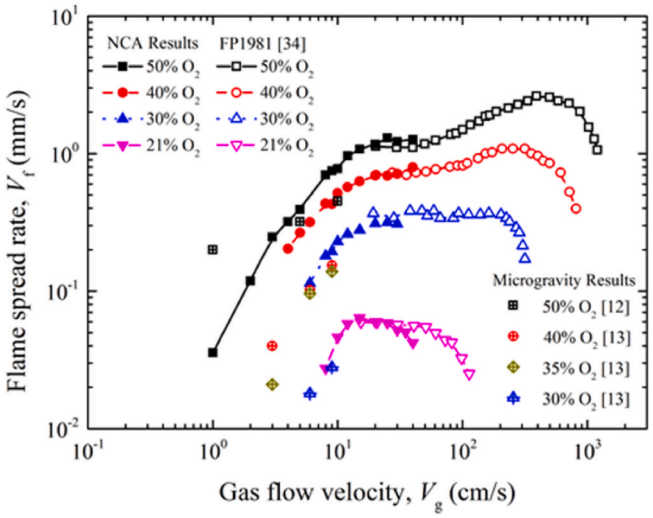

Fig. 6. Flame spread rate as a function of flow velocity under $P = 101$ kPa.

so the flame spread still decreases as the pressure is reduced but not as quickly. From the results of McAllister et al. [40], it is known that at 30% O_2 with 30 cm/s flow, the ignition delay time decreases by 22% when the ambient pressure is reduced from 101 kPa to 30 kPa. Cordova et al. [41] reported that the ignition delay time is independent of oxygen concentration when $X_{O2} > 25\%$. Therefore, it indicates that at 40% O_2, the ignition delay time may decrease with the same proportion as the pressure is reduced. However, the flame spread rate increases about three times when the pressure is increased from 35 kPa to 101 kPa, as is shown in Fig. 6. Then, it is inferred that the variation of ambient pressure on gas-phase heat conduction plays a more important role in flame spread rate. With the decrease of the ambient pressure, the flame extinguishes at higher oxygen concentration with high flow velocity due to the reduced gas-phase conduction.

At a low-velocity flow, the gas-phase heat conduction is small, and the radiation heat loss from the solid surface to the environment becomes increasingly important, making the flame spread rate sensitive to the opposed flow velocity. When the heat conduction reduced to a critical value, the uniform flame cannot be survived and separated into flamelets, and the flame extinguishes when further reduced. At a relatively large flow velocity, the flame spread rate increases with the increased flow velocity slowly. Accordingly, the transition flow velocity between the thermal regime and radiative regime increases with the reduced ambient pressure.

3.4.2. *Flame spread at a constant oxygen partial pressure*

At a constant P_{O2}, as the ambient pressure is reduced, the oxygen mass fraction Y_{O2} increases, and $Y_{O2} \sim P^{-1}$. According to Eq. (3), $T_f - T_{ig} \sim P^{-1}$. Considering that $\rho_g \sim P$, it can be inferred that $\dot{q}''_{fc} \sim P^{-1/2}$, and thus $t_{ig} \sim P^2$. Therefore, V_f will decrease with the increased ambient pressure. As the ambient pressure is reduced, the ignition delay time is decreased with the decreased gas density and increased oxygen mass fraction. In addition, the decreased gas density, increased oxygen concentration, and the corresponded increased flame temperature increase $\dot{q}''_{fc}$, and finally, promote flame spread. According to the results of McAllister et al. [40], at $P_{O2} = 21.3$ kPa, when the ambient pressure is reduced from 101.3 kPa to 21 kPa, the ignition delay time is reduced by 29.5%. In our work, the flame spread rate increases by more than 90%. It can be inferred that the effects of ambient pressure on both ignition temperature and gas-phase heat conduction play an important role in the flame spread process.

4. Conclusions

A low-velocity flow was produced by suppressing the buoyancy using a narrow channel apparatus in a low-pressure environment. Flame spread and extinction behavior were systematically studied. The main conclusions are drawn as follows:

(1) Under sub-atmospheric pressure with a constant flow velocity, the limiting oxygen concentration decreases with the increased pressure. There are two flame spread modes, i.e. uniform flame, which appears in the regions of flame spread away from the extinction, and flamelet, which appears with lower oxygen concentration and/or flow velocity. The flamelet region widens in terms of opposed flow at lower pressures. A flammability map around the quenching boundary was delineated, with the oxygen concentration and the gas flow velocity as two control parameters.

(2) In the flow velocity range tested. the flame spread rate increases with the increased flow velocity and two regimes are presented, which are the radiation-controlled and thermal-controlled regimes under sub-atmospheric pressure. The radiation-controlled regime enlarged with the decrease of the ambient pressure, and the thermal-controlled regime corresponds to a larger flow velocity.

(3) Low pressure affects the flame spread process by reducing the ignition temperature and gas-phase heat transfer. At a constant oxygen concentration, the reduced ignition temperature competes with the reduced heat conduction from the flame leading edge to the solid, and the heat transfer dominates the flame spread process, resulting in a decreased flame spread rate with

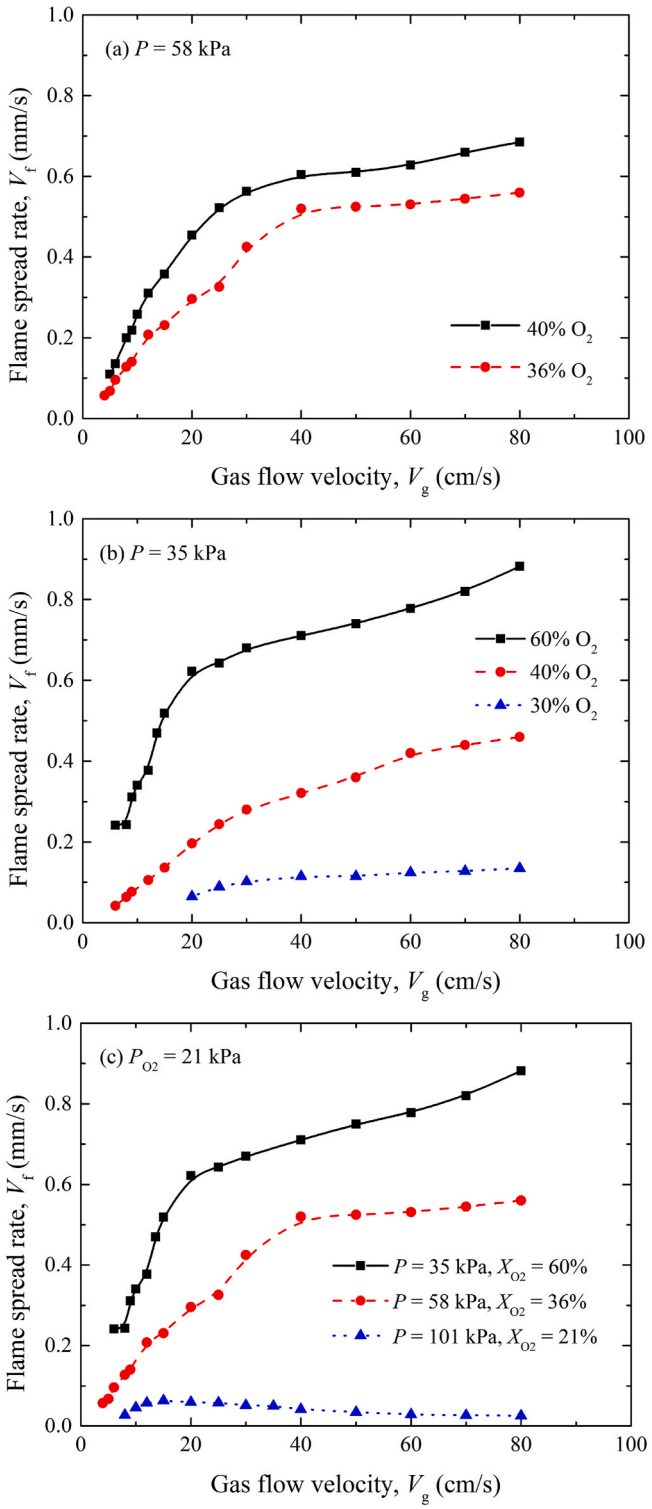

Fig. 7. Flame spread rate as a function of flow velocity under (a) $P = 58$ kPa, (b) $P = 35$ kPa, and (c) $P_{O2} = 21.3$ kPa.

reduced ambient pressure. When the oxygen partial pressure is constant, with the increase of the ambient pressure, both the increased ignition temperature and decreased heat conduction from the flame to the solid restrains the flame spreading process and results in a reduced flame spread rate.

Author Statement

Feng Zhu: Investigation, Methodology, Writing- Original draft preparation. Shuangfeng Wang: Conceptualization, Supervision, Project administration, Writing-review & editing. Zhanbin Lu: Investigation, Writing-review & editing. Chuanjia Wu: Investigation, Writing-review & editing.

Declaration of competing interest

The authors declare that they have no known competing financial interests or personal relationships that could have appeared to influence the work reported in this paper.

Acknowledgments

This work is supported by the National Natural Science Foundation of China, under Grant No. U1738117, the Strategic Pioneer Program on Space Science, Chinese Academy of Sciences, under Grant No. XDA04020410, and Opening Fund of State Key Laboratory of Fire Science (SKLFS) under Grant No.HZ2021-KF12.

References

[1] J.S. T'ien, H.Y. Shih, C.B. Jiang, H.D. Ross, F.J. Miller, A.C. Fernandez-Pello, J. L. Torero, D. Walther, Mechanisms of flame spread and smolder wave propagation, in: H.D. Ross (Ed.), Microgravity Combustion: Fire in Free Fall, Academic Press, 2001, pp. 299–418.

[2] O. Fujita, Solid combustion research in microgravity as a basis of fire safety in space, Proc. Combust. Inst. 35 (2015) 2487–2502, https://doi.org/10.1016/j.proci.2014.08.010.

[3] C. Lautenberger, J. Torero, C. Fernandez-Pello, Understanding materials flammability, in: Flammability Testing of Materials Used in Construction, Transport and Mining, 2006, pp. 1–21, https://doi.org/10.1533/9781845691042.1.

[4] G.A. Ruff, D.L. Urban, Technology development for fire safety in exploration spacecraft and habitats, Collection of Technical Papers - 45th, AIAA Aerospace Sciences Meeting 7 (2007) 4261–4274, https://doi.org/10.2514/6.2007-350.

[5] W. Liu, Z. Liu, J. Chen, Y. Peng, Selection of spacecraft atmospheric pressure regime for manned lunar exploration mission, Manned Spaceflight 22 (2016) 687–693, https://doi.org/10.16329/j.cnki.zrht.2016.06.004.

[6] R.A. Altenkirch, R. Eichhorn, A.R. Rizvi, Correlating downward flame spread rates for thick fuel beds, Combust. Sci. Technol. 32 (1983) 49–66, https://doi.org/10.1080/00102208308923652.

[7] F.A. Lastrina, R.S. Magee, R.F. McAlevy, Flame Spread over Fuel Beds : Solid-phase, Thirteenth Symposium (International) on Combustion, 1971, pp. 935–948.

[8] J. Gong, X. Zhou, Z. Deng, L. Yang, Influences of low atmospheric pressure on downward flame spread over thick PMMA slabs at different altitudes, Int. J. Heat Mass Tran. 61 (2013) 191–200, https://doi.org/10.1016/j.ijheatmasstransfer.2013.01.066.

[9] K. Zhao, X.D. Zhou, X.Q. Liu, L. Lu, Z.B. Wu, F. Peng, X.Y. Ju, L.Z. Yang, Prediction of three-dimensional downward flame spread characteristics over poly(methyl methacrylate) slabs in different pressure environments, Materials 9 (2016), https://doi.org/10.3390/ma9110948.

[10] S. Bhattacharjee, M.D. King, S. Takahashi, T. Nagumo, K. Wakai, Downward flame spread over poly(methyl)methacrylate, Proc. Combust. Inst. 28 (2000) 2891–2897, https://doi.org/10.1016/S0082-0784(00)80713-4.

[11] M. Thomsen, C. Fernandez-Pello, D.L. Urban, G.A. Ruff, S.L. Olson, On simulating concurrent flame spread in reduced gravity by reducing ambient pressure, Proc. Combust. Inst. 37 (2019) 3793–3800, https://doi.org/10.1016/j.proci.2018.05.004.

[12] S.L. Olson, U. Hegde, S. Bhattacharjee, J.L. Deering, L. Tang, R.A. Altenkirch, Sounding rocket microgravity experiments elucidating diffusive and radiative transport effects on flame spread over thermally thick solids, Combust. Sci. Technol. 176 (2004) 557–584.

[13] F. Zhu, Z. Lu, S. Wang, Y. Yin, Microgravity diffusion flame spread over a thick solid in step-changed low-velocity opposed flows, Combust. Flame 205 (2019) 55–67, https://doi.org/10.1016/j.combustflame.2019.03.040.

[14] C. Wu, X. Huang, S. Wang, F. Zhu, Y. Yin, Opposed flame spread over cylindrical PMMA under oxygen-enriched microgravity environment, Fire Technol. 56 (2020) 71–89, https://doi.org/10.1007/s10694-019-00896-8.

[15] T. Vietoris, J.L. Ellzey, P. Joulain, S.N. Mehta, J.L. Torero, Laminar diffusion flame in microgravity: the results of the MINITEXUS 6 sounding rocket experiment, Proc. Combust. Inst. 28 (2000) 2883–2889.

[16] D.L. Urban, P. Ferkul, S. Olson, G.A. Ruff, J. Easton, J.S. T'ien, Y.T. Liao, C. Li, C. Fernandez-Pello, J.L. Torero, G. Legros, C. Eigenbrod, N. Smirnov, O. Fujita, S. Rouvreau, B. Toth, G. Jomaas, Flame spread: effects of microgravity and scale, Combust. Flame 199 (2019) 168–182, https://doi.org/10.1016/j.combustflame.2018.10.012.

[17] J.S. Goldmeer, J.S. T'ien, D.L. Urban, Combustion and extinction of PMMA cylinders during depressurization in low-gravity, Fire Saf. J. 32 (1999) 61–88, https://doi.org/10.1016/S0379-7112(98)00017-4.
[18] Y. Zhang, P.D. Ronney, E.V. Roegner, J.B. Greenberg, Lewis number effects on flame spreading over thin solid fuels, Combust. Flame 90 (1992) 71–83, https://doi.org/10.1016/0010-2180(92)90136-D.
[19] T. Matsuoka, K. Nakashima, Y. Nakamura, S. Noda, Appearance of flamelets spreading over thermally thick fuel, Proc. Combust. Inst. 36 (2017) 3019–3026.
[20] K. Funashima, A. Masuyama, K. Kuwana, G. Kushida, Opposed-flow flame spread in a narrow channel: prediction of flame spread velocity, Proc. Combust. Inst. 37 (2019) 3757–3765, https://doi.org/10.1016/j.proci.2018.08.017.
[21] X. Huang, J. Gao, A review of near-limit opposed fire spread, Fire Saf. J. (2020), https://doi.org/10.1016/j.firesaf.2020.103141.
[22] Y. Uchida, K. Kuwana, G. Kushida, Experimental validation of Lewis number and convection effects on the smoldering combustion of a thin solid in a narrow space, Combust. Flame 162 (2015) 1957–1963.
[23] S. Hossain, I.S. Wichman, G.W. Sidebotham, S.L. Olson, F.J. Miller, Influence of gap height and flow field on global stoichiometry and heat losses during opposed flow flame spread over thin fuels in simulated microgravity, Combust. Flame 193 (2018) 133–144, https://doi.org/10.1016/j.combustflame.2018.02.023.
[24] S.L. Olson, F.J. Miller, S. Jahangirian, I.S. Wichman, Flame spread over thin fuels in actual and simulated microgravity conditions, Combust. Flame 156 (2009) 1214–1226, https://doi.org/10.1016/j.combustflame.2009.01.015.
[25] Y. Xiao, J. Hu, S.F. Wang, J.F. Zhao, A narrow channel experimental study on flammability characteristics of thermally thin fuels under simulated microgravity conditions, Yuhang Xuebao/Journal of Astronautics 31 (2010) 1877–1882, https://doi.org/10.3873/j.issn.1000-1328.2010.07.028.
[26] A. V Ivanov, Y. V Balashov, T.V Andreeva, A.S Melikhov, Experimental Flammability Verification in Space of Material NASA/CR-1999-209405, 1999.
[27] X. Zhang, Y. Yu, Experimental studies on the three-dimensional effects of opposed-flow flame spread over thin solid materials, Combust. Flame 158 (2011) 1193–1200, https://doi.org/10.1016/j.combustflame.2010.10.004.
[28] F. Zhu, Z. Lu, S. Wang, Flame spread and extinction over a thick solid fuel in low-velocity opposed and concurrent flows, Microgravity Sci. Technol. 28 (2016) 87–94, https://doi.org/10.1007/s12217-015-9475-4.
[29] F. Zhu, S. Wang, Z. Lu, A comparative study of near-limit flame spread over a thick solid in space- and ground-based experiments, Microgravity Sci. Technol. 30 (2018) 943–949, https://doi.org/10.1007/s12217-018-9655-0 ORIGINAL ARTICLE A.
[30] J.P. Holman, Heat Transfer, tenth ed., McGraw-Hill Higher Education, 2010.
[31] K. Wang, W. Xia, B. Wang, Y. Ai, W. Kong, Study on fire initiation of wire insulation by a narrow channel at low pressure, Microgravity Sci. Technol. 28 (2016) 155–163, https://doi.org/10.1007/s12217-016-9494-9.
[32] J.M. Pepper, F.J. Miller, S.L. Olson, I.S. Wichman, A study of the effectiveness of a narrow channel apparatus in simulating microgravity flame spread over thin fuels, in: 42nd International Conference on Environmental Systems 2012, ICES 2012, 2012, pp. 1–7, https://doi.org/10.2514/6.2012-3493.
[33] O. Zik, E. Moses, Fingering instability in solid fuel combustion: the characteristic scales of the developed state, Symp. (Int.) Combust. 27 (1998) 2815–2820.
[34] A.C. Fernandez-Pello, S.R. Ray, I. Glassman, Flame spread in an opposed forced flow: the effect of ambient oxygen concentration, Symposium (International) on Combustion 18 (1981) 579–589, https://doi.org/10.1016/S0082-0784(81)80063-X.
[35] S.L. Olson, P.V. Ferkul, J.S. T'ien, Near-limit flame spread over a thin solid fuel in microgravity, Symposium (International) on Combustion 22 (1989) 1213–1222, https://doi.org/10.1016/S0082-0784(89)80132-8.
[36] S.L. Olson, Mechanisms of microgravity flame spread over a thin solid fuel: oxygen and opposed flow effects, Combust. Sci. Technol. 76 (1991) 233–249, https://doi.org/10.1080/00102209108951711.
[37] J.G. Quintiere, Fundamentals of Fire Phenomena, John Wiley & Sons, 2006, https://doi.org/10.1002/0470091150.
[38] A.C. Fernandez-pello, The solid phase, in: Combustion Fundamentals of Fire, 1995, pp. 31–100.
[39] M.A. Delichatsios, Creeping flame spread: energy balance and application to practical materials, Symposium (International) on Combustion 26 (1996) 1495–1503, https://doi.org/10.1016/S0082-0784(96)80371-7.
[40] S. McAllister, C. Fernandez-Pello, D. Urban, G. Ruff, The combined effect of pressure and oxygen concentration on piloted ignition of a solid combustible, Combust. Flame 157 (2010) 1753–1759, https://doi.org/10.1016/j.combustflame.2010.02.022.
[41] J.L. Córdova, A.C. Fernandez-Pello, Convection effects on the endothermic gasification and piloted ignition of a radiatively heated combustible solid, Combust. Sci. Technol. 156 (2000) 271–289, https://doi.org/10.1080/00102200008947306.